ORNL/TM-2018/889

Analysis of FeCrAl cladding and UO_2 fuel including discrete and smeared cracks, and fuel relocation

Nuclear Technology Research and Development

Prepared for
U.S. Department of Energy
Nuclear Technology Research and Development Advanced Fuels Campaign
R. Sweet[1,2], A. Nelson[1], B. D. Wirth[1,2]
[1]Oak Ridge National Laboratory
[2]University of Tennessee Knoxville
June 28, 2018
M3NT-18OR020205031

Approved for public release.
Distribution is unlimited.

DISCLAIMER

This information was prepared as an account of work sponsored by an agency of the U.S. Government. Neither the U.S. Government nor any agency thereof, nor any of their employees, makes any warranty, expressed or implied, or assumes any legal liability or responsibility for the accuracy, completeness, or usefulness, of any information, apparatus, product, or process disclosed, or represents that its use would not infringe privately owned rights. References herein to any specific commercial product, process, or service by trade name, trade mark, manufacturer, or otherwise, does not necessarily constitute or imply its endorsement, recommendation, or favoring by the U.S. Government or any agency thereof. The views and opinions of authors expressed herein do not necessarily state or reflect those of the U.S. Government or any agency thereof.

SUMMARY

As UO_2 fuel heats during the rise to operating power in an LWR, the fuel pellets begin to fracture due to thermal stresses arising due to the temperature profile radially across the fuel. As the fuel fractures, it expands diametrically, reducing the fuel cladding gap and improving the heat transfer characteristics of the fuel. By increasing the effective fuel diameter, gap closure is expected to occur much sooner and greater stresses are expected to form in cladding.

In order to assess the diametral expansion of UO_2 fuel pellets due to fracture and its subsequent effect on the formation of stresses in the cladding, explicit fracture models are compared using the BISON fuel performance code.

This milestone report describes the results of analyses FeCrAl cladding fueled with UO_2 pellets. Discrete and smeared cracks as well as fuel relocation are taken into account in this analysis, and points to the need for further work in order to correctly model the fuel mechanics which ultimately controls the stresses that develop in the fuel cladding.

Table of Contents

List of Tables

List of Figures

Analysis of FeCrAl cladding and UO_2 fuel including discrete and smeared cracks, and fuel relocation

1. INTRODUCTION

Our previous work has demonstrated the use of the BISON fuel performance code to assess FeCrAl cladding, and shown that the mechanical behavior of the cladding after gap closure is very sensitive to models associated with the fuel compliance (Sweet et al., 2018). This emphasizes that accurately modeling the fuel mechanics is critically important, since this controls the diametric expansion and elastic-plastic response of the fuel that determines the cladding mechanical response and the onset of gap closure.

As the temperature of UO_2 fuel is increased during reactor power ascension, significant thermal stresses form across the fuel pellet due to differential thermal expansion as a result of the steep radial temperature gradient that forms (Olander, 1976). These thermal stresses are tensile in the fuel periphery and transition to compressive approaching the fuel center. These large tensile hoop stresses initiate radial cracks in the fuel, starting near the fuel periphery and propagating inward. If the power in the fuel is then quickly decreased after the fuel has been plastically deformed, the stress profile is changed and the central region of the fuel transitions to a tensile state. This allows circumferentially-oriented cracks to form at radial distances about 30% from the fuel centerline (Rashid, 1974).

The formation of fuel cracks increase the apparent fuel diameter as the fragments are free to expand and eventually move outward toward the cladding (Williford et al., 1980). The movement and dispersal of these fragment is a phenomenon known as ‘relocation’. As fuel temperatures are increased, more cracks are expected to form in the fuel, increasing the effect of relocation (Oguma, 1983). Currently used relocation models for fuel performance calculations are empirically-derived and include, along with fracture, other effects that alter the fuel cladding gap evolution, such as the eccentric location of fuel pellets in the gap region, which may occur without constraints to hold the fuel pellets perfectly aligned and centered (Cunningham et al., 1979).

Fracture can affect many aspects of integral fuel rod performance. While this study is focused on fuel temperatures and expansion, fracture may also increase the ability of the fuel to release fission gas to the fuel rod gap and alter the cladding stress state (Maki and Meyer, 1978). As radially-oriented cracks form, they allow the fuel to expand; reducing the fuel cladding gap and lowering fuel temperatures. Circumferential cracks, however, may impede the heat transfer from the core of the fuel to the cladding because the fuel has a higher thermal conductivity than the fill gas. A short study has been performed, as discussed in Appendix A, demonstrating that a diametral fuel increase due to cracking will reduce the fuel temperatures. This study, however, only evaluates the temperature distribution and does not consider the coupled thermo-mechanical effects or material property changes due to fuel burnup.

Cracking may also increase the release of gaseous fission products to the fuel rod plenum by increasing the free surface area to which the products may diffuse and by directly opening fission gas bubble networks intersected by the surface of the cracks. By providing a free pathway to the fuel rod gap/plenum, the fission gas inventory is expected to increase and eventually alter the gap heat transfer characteristics in the fuel rod. Although this effect is not considered in the current analysis, it is expected to alter fuel temperatures, at least before gap closure occurs.

As power in the fuel is continually cycled during operation, fuel fragments are slowly able to migrate outward radially. This ‘ratcheting’ behavior of the fuel fragments generally has a diminishing effect with an increasing number of power cycles and occurs until contact is established between the fuel and cladding (Rashid, 1974). Fuel fragment relocation and subsequent crack closure leads to the development

of an asymmetric fuel surface in contact with the cladding. Previous work has been performed to demonstrate the tendency for large cladding stresses to form as gap closure occurs with fuel containing cracks (Gittus, 1972) and defects (Capps et al., 2016). Determining the mechanical response of the cladding after gap closure with open cracks in the fuel requires accurate calculation of the coefficient of friction between the fuel and cladding and, thus, is not considered here.

Several models have been proposed to include the effect of fracture into fuel performance simulations. These include a variety of numerical methods to approximate the fuel expansion and in some cases, the fuel property evolution.

Novel fracture models have been developed to incorporate cracking as an alteration of the bulk fuel thermal and elastic properties. This can be performed by determining whether the fuel has reached a fracture stress, and if it has, adjusting the directional (or isotropic) elastic properties based on the direction and number of cracks assumed to have formed (Jankus and Weeks, 1972). Additionally, similar methods have been suggested by applying an "effective" elastic modulus and modeling the apparent diametral expansion as an extension of the thermal expansion calculation (Williford, 1982).

A more explicit model, the smeared cracking model, is used in finite-element analysis to determine the elastic behavior of the fuel on an element-by-element basis (Rashid et al., 2004). If the single element is specified as cracked, the elastic properties of the element are reduced. This allows stress concentrations to develop in the surrounding elements as the element loses strength, and as such, a cracking pattern is able to from in the fuel. This provides a more accurate, however, much more computationally intensive fracture model.

In order to simplify the computational requirements of these models while still applying the stress relief from fracture, discrete cracking models have also been utilized. These allow prescribed discrete cracks to be applied directly to the fuel mesh before the simulation begins.

Other models simply include the diametral expansion due to fuel fracture. This can be accomplished by applying a radial strain directly to the fuel column based on the linear heat rate, as used in many fuel performance codes including BISON. Fuel relocation not only increases the diameter of the fuel, reducing the time before the onset of gap closure, by reducing the gap thickness, but it also reduces the fuel temperatures. The models used in this analysis utilize some combination of the characteristics from the aforementioned fracture methods.

This report describes efforts to determine the effect of neglecting explicit fracture models on the calculation fuel expansion and compliance. Section 2, documents the fracture models considered in this analysis. Section 3 reports the results of a comparison between these fracture models for a well-characterized test fuel rod. Section 4 extends this analysis by applying these models to a FeCrAl cladded fuel rod using a representative BWR fuel rod geometry. Section 5 provides an extension of the FeCrAl cladded fuel rod analysis using constant operating conditions. The findings of this analysis and possible enhancements to these models are further discussed in Section 6.

2. Fuel Mechanics Models

The current implementation of fuel relocation in BISON involves an empirical model that applies a radially-oriented strain based upon the local linear power, the cold fuel diameter and gap, and the fuel burnup. While this method predicts relocation well in specific instances, it artificially changes the fuel diameter to accomplish it. For example, by not relieving the stress during fracture, the response of other plasticity models, such as creep, is altered. In order to model fuel pellet relocation more mechanistically, explicit fracture models need to be considered. As previously mentioned, these may consist of relaxing

the elastic stiffness of specific elements in the finite-element mesh as they surpass the material's fracture strength, known as smeared cracking (Figure 1(a)), or prescribing cracks directly to the finite element mesh, known as discrete cracks (Figure 1(b)).

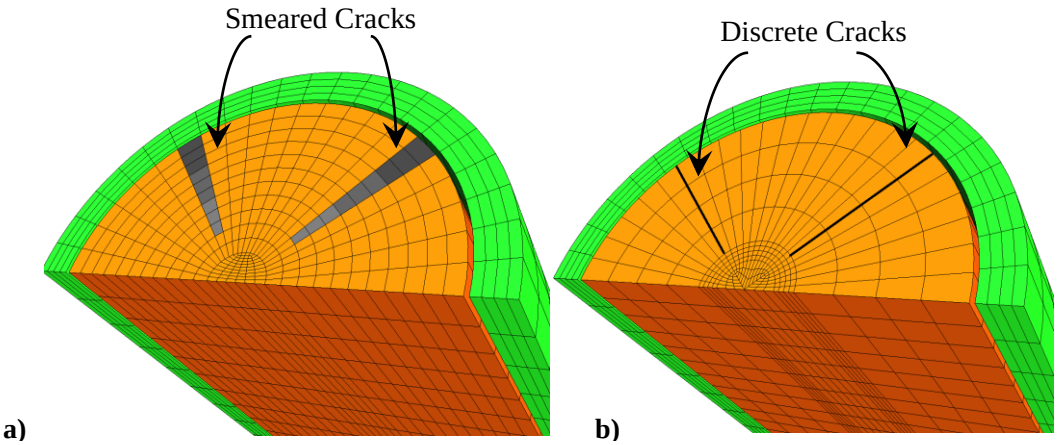

Figure 1. 3D illustration of two different fracture models commonly considered in finite element fuel performance codes. Smeared cracking (a) consists of relaxing elastic constant of the material as the stress in those elements surpasses the fracture strength. Discrete cracking (b) consists of prescribing cracks directly to the geometry.

Figure 2 shows a comparison, performed using BISON (Williamson et al., 2012), of the measured and calculated fuel centerline temperatures using relocation and smeared cracking models for a specified linear heat generation rate. It is important to note that the details of fuel creep in this assessment were not immediately available. Although this shows that smeared cracking, in this instance, does not possess the same reduction in temperature that the relocation model does, it does demonstrate that there is an impact on fuel temperature. This may indicate that other important phenomena beyond fracture may also have a significant contribution to the fuel diametral strain.

In order to more accurately model the mechanical behavior of UO_2 fuel leading up to and during pellet-cladding mechanical interaction using the BISON fuel performance code, a comparison of several fuel mechanics models has been performed. This analysis consists of a comparison between fracture models and the fuel relocation model with experimental data to determine the effect of explicitly modeling fuel fracture on cladding stress state and expansion. Along with the fuel creep model, which was analyzed separately (Sweet et al., 2018), models currently implemented in BISON include fuel relocation, smeared cracking, isotropic softening.

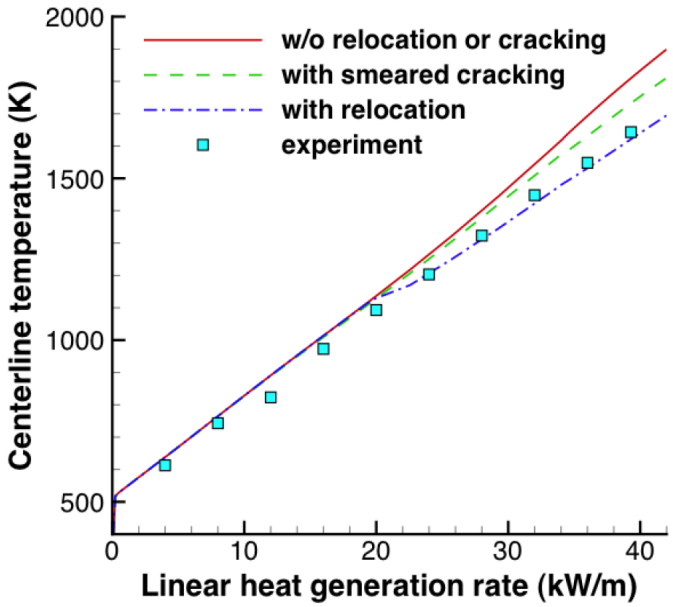

Figure 2. The predicted fuel centerline temperature as a function of linear heat generation rate for varying fuel mechanics models, as compared to experimental measurements (blue squares). The fuel temperature increases nearly linearly with the linear heat generation rate until the fracture models alter the fuel expansion, starting at nearly 20 kW/m. The models with greater fuel expansion experience lower fuel centerline temperatures. [Reproduced from (Williamson et al., 2012)]

2.1 Fuel Relocation

The fuel relocation model used in this analysis is based on the ESCORE model developed by EPRI (Rashid et al., 2004), although it was subsequently modified An uncertainty quantification analysis performed by (Swiler et al., 2013) determined that, for a specific subset of fuel rods (IFA-431 and IFA-432) from the Halden test reactor, the most likely onset of fuel relocation occurred at a much lower linear heat rate than the ESCORE model indicated. In order to accommodate this, changes were made to the activation thresholds of the model and their functional dependence on the linear heat rate. The result of this is considered the 'Modified ESCORE' model (Hales et al., 2014). Equation 1 shows the general function for the change in the diameter relative to the initial fuel diameter.

$$\left(\frac{\Delta D}{D_O}\right) = 0.80 \cdot Q_r \cdot \left(\frac{G_t}{D_O}\right) \cdot (0.005 \cdot Bu^{0.3} - 0.20 \cdot D_O + 0.3) \quad (1)$$

In Eq. (1), ΔD is the change of the fuel diameter due to relocation (inches), D_O is the initial, as-fabricated, cold fuel diameter (inches), G_t is the initial, as-fabricated, cold diametric fuel rod gap (inches), Bu is the average fuel burnup (MWd/MTU), and Q_r is a dimensionless piecewise function based on the linear heat rate. Equation 2 describes the Q_r function for the Modified ESCORE model and Equation 3 describes the Q_r function for the unchanged ESCORE model.

$$Q_r = \begin{cases} 0 & for\ q' \leq 1.524 \frac{kW}{ft} \\ \frac{2 \cdot q'}{14} & for\ 1.524 \frac{kW}{ft} < q' \leq 14 \frac{kW}{ft} \\ \frac{q' - 10}{2} & for\ 14 \frac{kW}{ft} < q' \end{cases} \quad (2)$$

$$Q_r = \begin{cases} 0 & for\ q' \le 6\frac{kW}{ft} \\ (q'-6)^{\frac{1}{3}} & for\ 6\frac{kW}{ft} < q' \le 14\frac{kW}{ft} \\ \frac{q'-10}{2} & for\ 14\frac{kW}{ft} < q' \end{cases} \quad (3)$$

In Eqs. (1-3), Q_r is a dimensionless piecewise function and q' is the linear heat rate in kW/ft.

The difference between these models are the threshold linear heat rate where the onset of relocation begins, and the functional dependence of the Q_r term in the intermediate expansion region. The modified ESCORE model has a much lower activation energy at ~1.524 kW/ft (~5 kW/m) compared to the original model which begins at ~6 kW/ft (~19.7 kW/m), targeted toward simulating fracture at lower linear heat generation rates. Likewise, the functional dependence for the linear heat rate during the onset of relocation is also changed from a cubic term to a linear dependence. Figure 3 shows the difference in the amount of fuel radial expansion expected between these two models for a typical PWR fuel geometry at three separate fuel burnups and a range of linear heat rates. This shows the large difference between the two models over the 5 – 20 kW/m range and a relatively small difference after ~25 kW/m. Although the Modified ESCORE model was used in this analysis, because of the limited size of the data used in the model calibration, it is uncertain whether consideration should be continued.

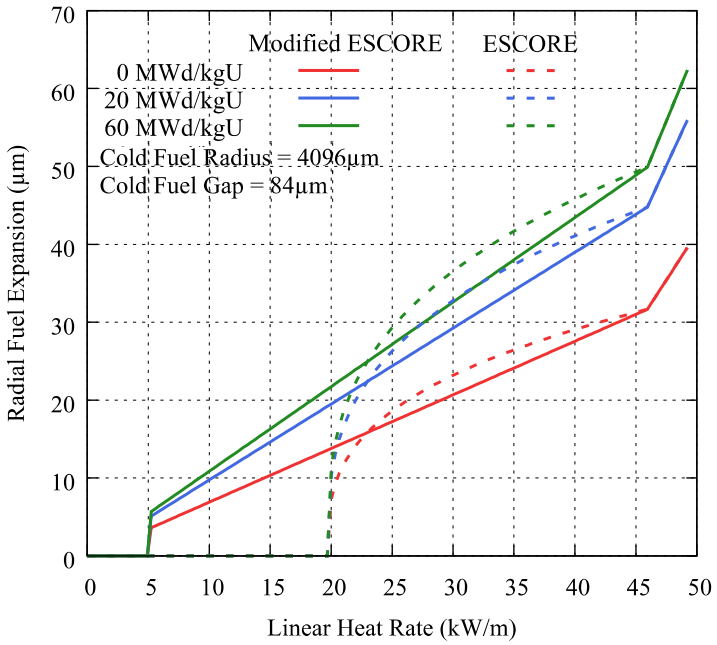

Figure 3. The original (dashed) and modified (solid) relocation models calculate a large difference in the radial fuel expansion between 5 – 20 kW/m for a typical PWR sample geometry. The modified ESCORE model features a much lower threshold where relocation is expected to begin (~5 kW/m) and a linear radial expansion as a function of linear heat rate.

2.2 Smeared Cracking

In order to simulate explicit fracture using a smeared cracking model, a fracture strength model for UO_2 from the MATPRO library (Hagrman et al., 1995) has been implemented. The expression, shown in Equation 4, describes the out-of-pile temperature and density dependent fracture strength as no in-pile data is currently available.

$$\sigma_f = 1.7 \times 10^8 \left[1 - 2.62(1 - D)\right]^{\frac{1}{2}} e^{\left(-\frac{1590}{8.314 \cdot T}\right)} \quad (4),$$

where σ_f is the fracture strength (Pa), D is the fractional density (fraction of theoretical density), and T is the temperature (K). This is applied for fuel temperatures up to 1000K; beyond this temperature the strength is assumed to be constant ($\sigma_f = \sigma_f(1000K)$). In order to enhance the expected crack propagation through the fuel, a statistical approach was taken by seeding the fuel mesh with a normal distribution and applying the fracture stress. Equation 5 provides the probability density function for a normal distribution with an average value of zero.

$$f(x) = \frac{1}{\sqrt{2\pi\mu^2}} e^{\left(-\frac{x^2}{2\mu^2}\right)} \quad (5),$$

where f(x) is the probability function for a normal distribution centered at zero with a standard deviation (μ) of 19 MPa. After each element is seeded with a sample from the probability function, the temperature and density dependent fracture stress is combined to give each element in the fuel mesh a unique, normally distributed temperature dependent fracture strength. Although not considered in this analysis, including a grain size dependence on the fuel fracture strength, as described by (Hagrman et al., 1995), may additionally improve fidelity for fuel fracture. Figure 4 shows a sample distribution of the fracture strength over temperature for 95% TD UO_2 fuel. The shaded area in the figure shows the range of a single standard deviation from the average.

An example mesh using the r-θ coordinate simulation capability in BISON, similar to those used in the following analysis, is shown in Figure 5. It should be noted that the fracture strength is declared as an isotropic value within the finite-element fuel mesh.

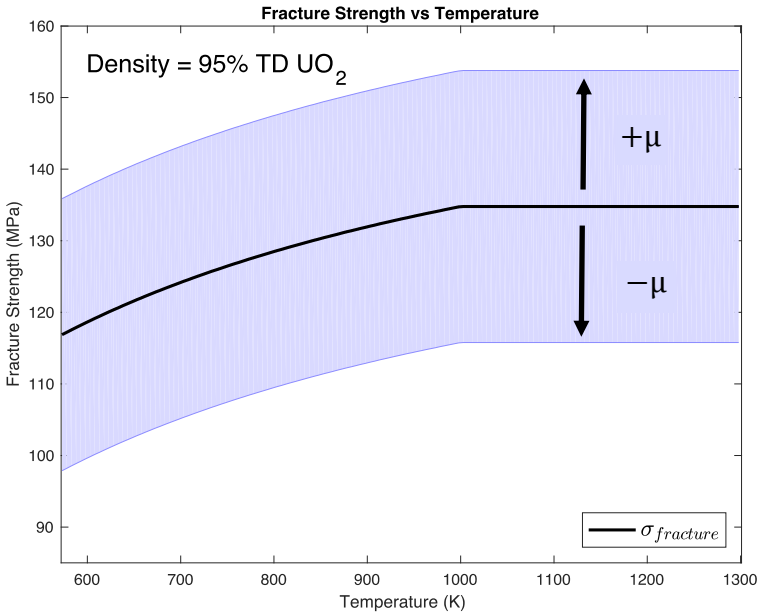

Figure 4. The fracture strength of UO_2 is shown as a function of temperature, based on out-of-pile measurements, as no in-pile data is currently available. The standard deviation of the fracture strength

(shaded) is quite large as UO_2 undergoes brittle fracture. Above 1000 K, the fracture strength is assumed to be constant.

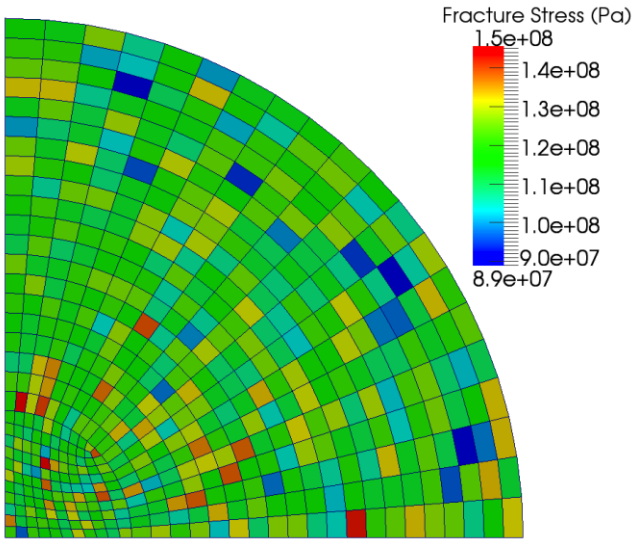

Figure 5. This quarter fuel pellet r-θ mesh demonstrates the distribution of the isotropic fracture strength at each element.

In order to simulate fracture in the fuel, a smeared cracking model (Rashid, 1968) is used. In this model, the elastic properties in an individual direction are reduced based on the crack strain or number of times an element cracks, after the fracture stress has been reached in that specific element. Because of the nonlinearity introduced into the system, a truly abrupt cracking model (where the elastic properties are immediately reduced to zero) reduces the ability of the fuel performance code solver to find convergence. This makes it extremely difficult to determine the solution, and thus alternative models are considered. The smeared cracking model implemented in BISON (Hales et al., 2014) is currently based on an exponential softening curve (Equation 6). In this model, after the aforementioned fracture strength is reached, the elastic properties of an element are exponentially reduced as the crack strain is increased. This allows the element to retain elastic properties initially; and as the crack begins to open, these are greatly reduced.

$$\sigma = \sigma_f \cdot \left(\sigma_{residual} + (1.0 - \sigma_{residual}) \cdot e^{\left(\frac{-E*\beta}{\sigma_f} * (\varepsilon_{max} - \varepsilon) \right)} \right) \quad (6),$$

where σ is the stress in the element, σ_f is the isotropic fracture strength in the element, $\sigma_{residual}$ is the user provided residual stress in a specified direction, E is the elastic modulus, ε_{max} is the maximum strain in that specific element, β is a user specified softening factor, ε is the crack strain in the crack direction. For this analysis, the residual stresses in the axial direction and the radial plane are set to zero to allow a continued reduction of the elastic properties for each cracked element. The value of β is assumed to be one, meaning the initial slope of the exponential model after an element has cracked is equal to the negative elastic modulus.

To further improve the robustness of the solver mechanics, an additional calculation of the fuel stress based on the number of times an element 'cracks' can be used. In this power-release model (shown in

Equation 7), the elastic properties are reduced to 1/3 of the current properties every time the fuel reaches the fracture stress. The fracture stress, in turn, is based on the exponential softening curve, so after each crack forms, it becomes easier to reach the fracture strength again and reduce the elastic properties in that element, allowing the crack to open further. Thus,

$$\sigma = \left(\frac{1}{3}\right)^n \cdot E \cdot \varepsilon \quad (7),$$

where σ is the stress in the element, E is the elastic modulus, n is the number of cracks in that element, and ε is the strain in that element.

Figure 6 shows a comparison of the stress-strain exponential and power release models. The main difference between the exponential (a) and power-release (b) models is how the mechanical properties are relaxed after the fracture strength has been reached. The exponential release model exponentially softens the fuel perpendicular to the crack as the crack strain increases. The power release model decreases the elastic modulus to 1/3 of the original value and utilizes the exponential strain softening curve to calculate the new fracture strength. This shows the relatively smooth release of the elastic properties for the exponential model.

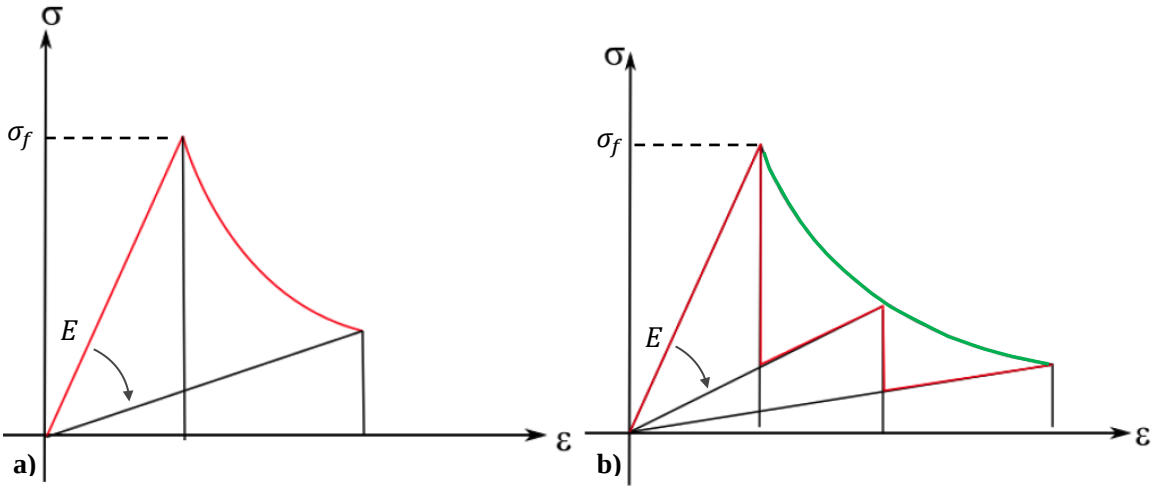

Figure 6. a) Exponential versus b) power release model, in which the red lines denote the current element stress based on the strain. For the exponential model the elastic modulus is softened gradually, while for the power release model this occurs suddenly. The green line denotes the strain softening curve from the exponential model. [Reproduced from (Liu and Rashid, 2017)].

2.3 Mesh Topography-Based Fracture

To compare against the smeared cracking models, another explicit fracture model, the discrete crack, is considered. Unlike smeared cracks, the mechanical properties of the fuel using the discrete crack remain unchanged during the simulation. Instead, cracks are prescribed to the mesh based on observed crack properties in the fuel before the simulation begins. Although this is a poor assumption for the early stages of the simulations, before fracture would normally occur, it is generally much less resource intensive to get a converged solution. A 90˚ r-θ mesh used in this analysis is shown in Figure 7 demonstrating the locations and geometry of the cracks in the fuel pellet. For this analysis, it is assumed eight cracks exist in the fuel (two of which are on the plane of symmetry, one in the center) which transverses the fuel at

70% of the fuel radius. The initial crack width, which is limited by the mesh generation software, is approximately 0.5˚. Cracks located on the symmetry plane are only .25˚ from the axis boundary.

An example of the hoop stress distribution in a fuel pellet with discrete cracks during a ramp to operating power is shown in Figure 8. In this demonstration, the hoop stress is reduced in the fuel pellet periphery along the cracks because the fuel is allowed to move. As the fuel is heated and expands during a power ramp, thermal stresses form in center of the cracked fuel lobes, away from the crack surfaces. Due to the increased temperature and thermal expansion at the center of the fuel, the core of the pellet is in a compressive stress state. The fuel periphery is in a tensile stress state because the core of the fuel pellet experiences more thermal expansion from the temperature gradient and expands the fuel.

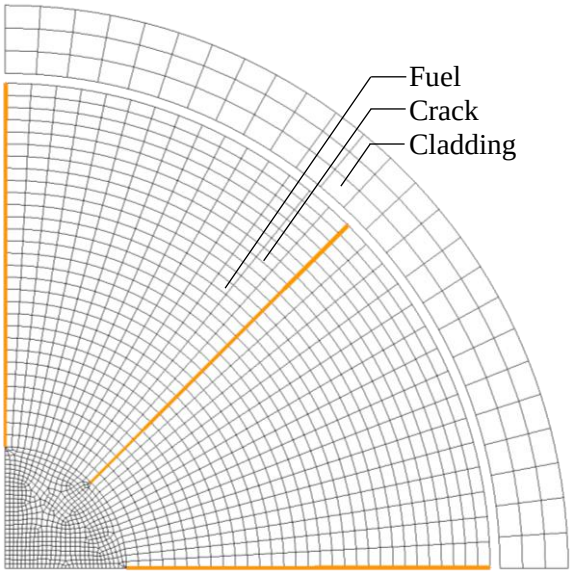

Figure 7. Finite element mesh showing the geometry used in the discrete crack fuel simulations. The cracks are noted in yellow and penetrate 70% of the fuel radius.

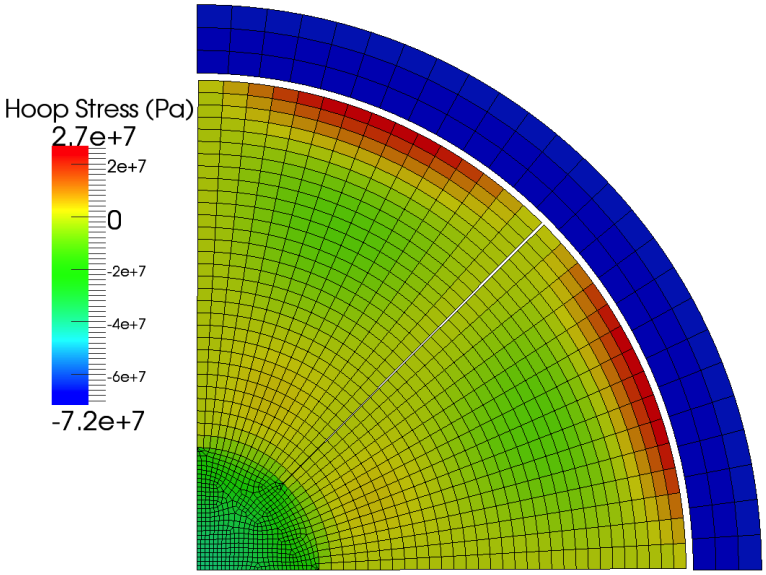

Figure 8. Distribution of hoop stress (color scale indicated spanning -72 to +27 MPa) within the fuel and cladding following an increase to a power level of 10 kW/m.

2.4 Isotropic Softening

Another approach to quickly modeling fuel fracture, implemented in BISON (Hales et al., 2014), is the use of a linear heat rate-based softening of the elastic properties of the fuel. As the fuel develops thermal stresses from the strong radial temperature gradients, the fuel is expected to fracture. A simple assumption can then be made to determine that if the fuel reaches a certain linear heat rate, considering the geometry to be the same, then the fuel will fracture. This work is similar to that of (Oguma, 1983), which extrapolates this cracking behavior to large linear heat rates by applying more radial cracks in each of the crack lobes, and eventually applying a circumferential crack. An illustration of this, reproduced from Oguma, is shown in Figure 9. This demonstrates the assumed step behavior of increasing fracture in UO_2 with an increasing linear heat rate. While this approach is difficult to apply to different fuel geometries (in the case of FeCrAl with much larger fuel pellets), it is also much less computationally intensive than smeared cracking models that calculate fracture based on a stress-based criterion.

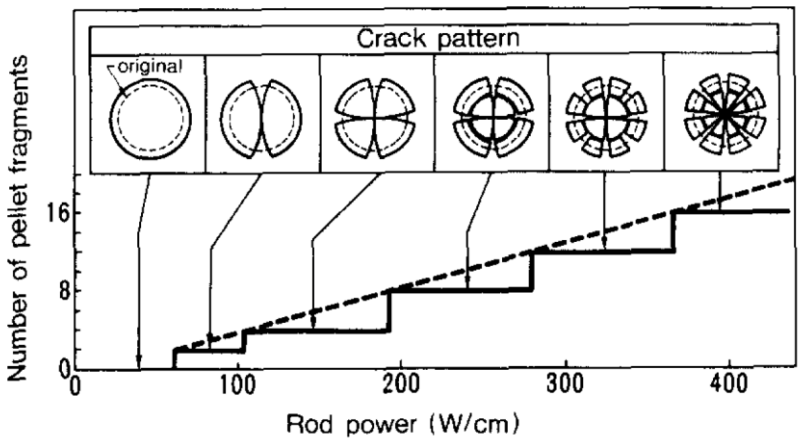

Figure 9. The expected crack patterns resulting from increases in the fuel linear heat rate. This increase in the number of cracks is predicated on the relationship between the thermal stresses that form across the fuel pellet and the fuel temperatures as the fuel linear heat rate increases, as reproduced from Ref. (Oguma, 1983).

In this isotopic softening model, the number of cracks is calculated using the linear heat rate, as shown in Equation 8. This equation is the result of fitting cracked fuel data. As shown in Figure , this model was fit to the experimental data of Walton and Husser, which was intended for use in a mechanistic fracture/relocation model for the FUMAC and TACO fuel performance codes (Walton and Husser, 1982). Thus,

$$N_{cr} = 1 + 10 \cdot \left(1 - exp\left(-\frac{LHR - 5}{21}\right)\right) \quad (8),$$

where N_{cr} is the number of cracks, and LHR is the fuel rod average linear heat rate in kW/m. In this equation, the first crack is assumed to form at 5 kW/m and the maximum number of cracks is assumed to be 11. Figure 10 shows a comparison between this model and the original model proposed by Oguma. Both of these models agree well with their respective data sets, although there is only limited data from

Oguma for high linear heat rates. Because the fuel geometries are not available, this comparison is somewhat difficult to extrapolate to different fuel pellet sizes.

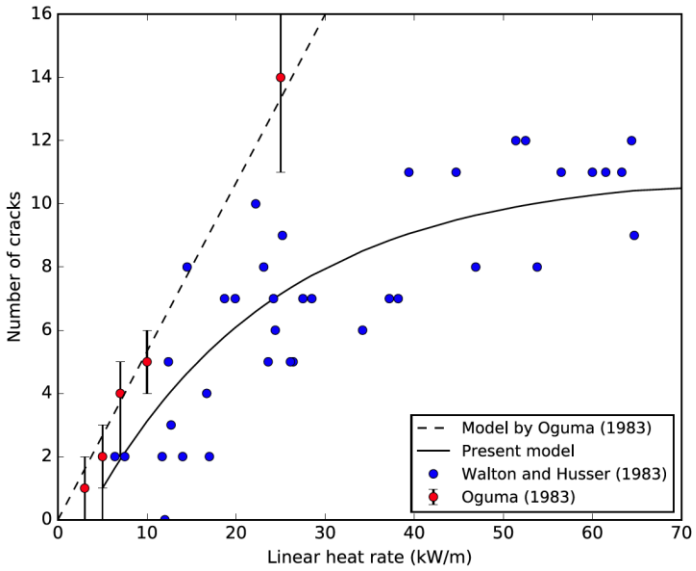

Figure 10. The number of cracks versus linear heat rate from the present model uses data from (Walton and Husser, 1982) as opposed to the Oguma model(Oguma, 1983), as reproduced from Ref. (Hales et al., 2014).

In order to reduce the elastic properties of the fuel as it fractures, the following reduction factors are applied to the elastic modulus (Equation 9) and Poisson's ratio (Equation 10) based on the number of cracks calculated in Equation 8, as:

$$f_{el} = \left[\left(\frac{2}{3}\right) \cdot \frac{(2-\nu)}{(2+\nu)(1-\nu)}\right]^{N_{cr}} \quad (9),$$

where f_{el} is the ratio of the elastic modulus remaining after cracking, and is the ν is Poisson's Ratio of the fuel. For these simulations the Poisson's Ratio of the fuel is calculated using a relation from the MAPTRO library currently implemented in BISON. The reduction factor for the fuel Poisson's Ration is calculated as:

$$f_{\nu} = \frac{1}{2^{N_{cr}} + \nu \cdot (2^{N_{cr}} - 1)} \quad (10),$$

where f_{ν} is the ratio of the remaining Poisson's ratio. Figure 11 shows these reduction factors as a function of the number of cracks in the fuel. For this simple comparison, the Poisson's ratio of the fuel is assumed to be 0.35. This shows the somewhat rapid loss of the elastic properties for the first few cracks formed at relatively low fuel linear heat rates. For example, at 10 kW/m it is assumed that ~3 cracks will be formed, reducing the elastic modulus to ~30% and Poisson's ratio to ~10%. Likewise, for an average linear heat rate of 20 kW/m, ~6 cracks are expected to be formed, reducing the elastic modulus to ~15% and Poisson's ratio to ~1%. These reduction factors show how quickly the elastic properties of the fuel are reduced after relatively few cracks (which occurs at a relatively low LHR).

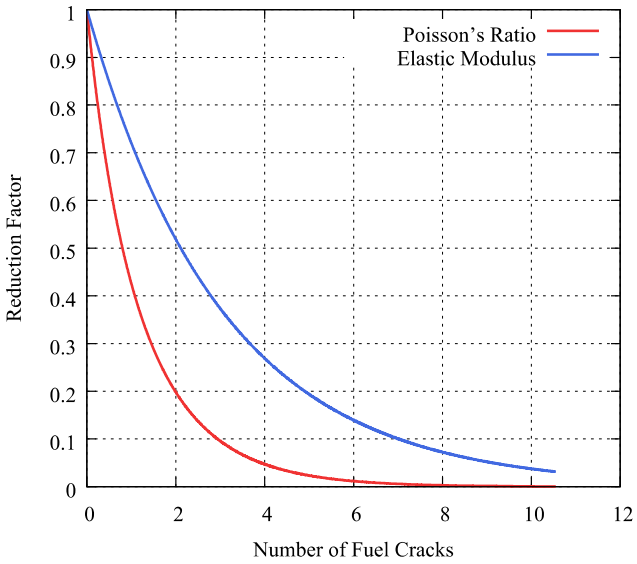

Figure 11. The reduction factors for the isotropic softening model as a function of the number of cracks formed in the fuel, which are dependent on the linear heat rate in the fuel.

To summarize, for this analysis several different methods of simulating explicit fracture in the fuel are considered. These consist of: the Modified ESCORE relocation model which empirically applies a radial strain to the fuel at a specified linear heat rate; the exponential and power-release smeared cracking models which reduce the elastic properties in a single finite-element based on the crack status and strain; the discrete meshed crack method which has an assumed crack number and geometry contained in the mesh for the finite-element simulation; and the isotropic softening model which relaxes the elastic properties of the fuel based on the number of cracks in the fuel, which is calculated by the rod average linear heat rate. The MATPRO fuel creep model (the original model, as it is implemented in (Hagrman et al., 1995)), is also considered in this analysis, implemented either as a standalone plasticity model or in conjunction with the fracture models.

3. OSIRIS Rod H09 Results

To compare the accuracy of each of the fracture models, the OSIRIS Rod H09 was chosen as a benchmark case from International Fuel Performance Experiment (IFPE) Database (Sartori et al., 2010). This rod was chosen, in particular, because it is a full-length Zircaloy cladded fuel rod, the reactor operating conditions are documented, and data from the post irradiation examination contains axial profilimetry. These diametral measurements are used to compare the final diameter of the fuel rod with predictions from BISON simulations.

In order to simulate this test rod, the geometry is generated from specifications in the IFPE database, shown in Table 1, using a quarter of an r-theta slice of the fuel rod. Figure 12 shows the fuel rod mesh considered in these simulations. Because of the symmetry in this mesh, only a quarter is used (with appropriate boundary conditions) in an effort to reduce the computational requirements. The geometry and reactor conditions for the OSIRIS Rod H09 are representative of a standard PWR.

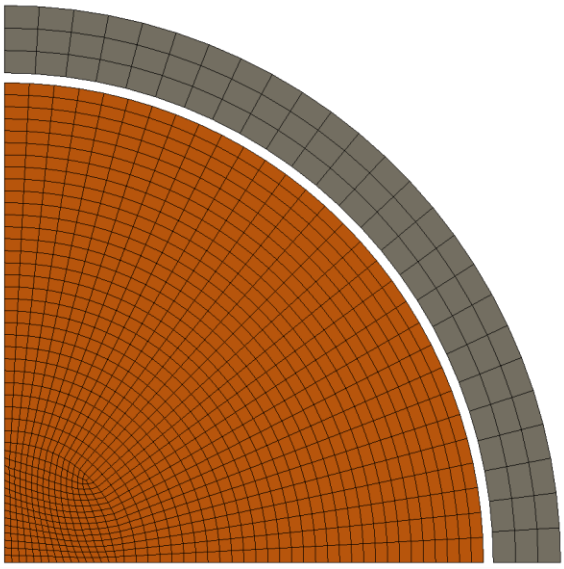

Figure 12. The quarter-rod r-theta coordinate geometry shows the fuel and cladding mesh density used in these simulations.

The r-theta geometry used in these simulations is a slice through the fuel rod, and as such, the conditions at that axial location of the slice can alter the results. For these simulations, the fuel rod operating conditions and the end-of-life fuel rod diameter are generated from the highest power axial location along the fuel rod.

Table 1. OSIRIS H09 Fuel Rod Geometry Specification

Cladding Type	Fuel Radius (μm)	Gap Thickness (μm)	Cladding Thickness (μm)
Zircaloy	4095	84	575

The power history for the OSIRIS H09 test rod is shown in Figure 13. There are four significant features in the power maneuvering of this test rod that are expected to cause fuel cracking from the development of thermally-induced stresses. The first occurs during the rise to operating power, where the fuel increases to ~23 kW/m over approximately (200 hours). It is expected that such a rapid increase in the fuel temperatures over a relatively short time will lead to the bulk of the cracking behavior in the fuel. The second is the power reduction at nearly ~1.6 years. When the fuel is operated at high temperatures for long periods of time, stresses in the fuel will relax due to thermal and irradiation creep. If the fuel power is suddenly decreased, large circumferentially-oriented cracks develop from the large radial stresses that form as the core of the fuel contracts. After this sharp decrease in power, there is a corresponding ramp up in power. Again, during large power cycles more radial cracks are expected to form. Finally, as the fuel temperatures are decreased during reactor shutdown at the end of the power history, large circumferential cracks may form. It should be noted that shutdown between reactor cycles was not documented in the power history provided in the IFPE database. This is expected to have a similar effect on fuel fracture as the initial reactor startup and shutdown.

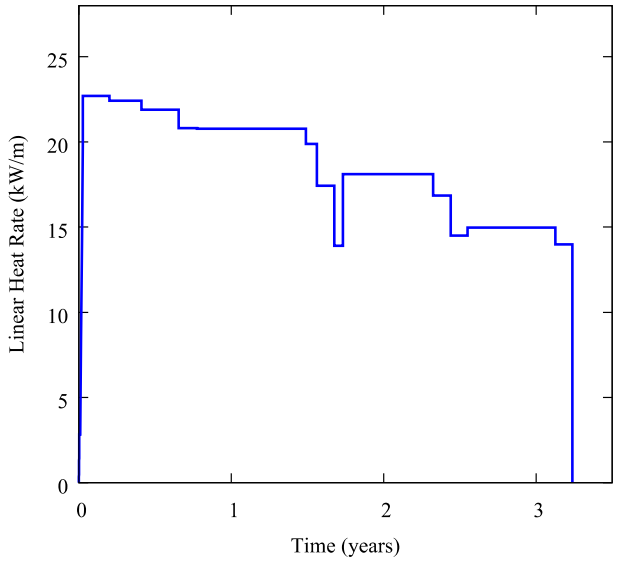

Figure 13. The power history, as reported in the IFPE Database for the OSIRIS H09 test fuel rod, shows several important features of the fuel rod operation including the rapid rise to 20 kW/m and a sharp decrease in power at ~1.6 years.

This particular fuel rod in the OSIRIS test suite was operated in a PWR for four cycles. Fuel and reactor properties are shown in Table 2. Because these r-theta geometries do not have a discrete plenum included in the mesh, it is difficult to accurately calculate the temperature and pressure of the gas in the gap/plenum. In these simulations, the gas pressure is only affected by the calculated gap temperature, there is no volumetric change from gap closure or pressure increase from fission gas release. This is performed because there is not a discrete temperature calculation for the fuel rod plenum in the r-theta geometry.

Table 2. OSIRIS H09: Reactor and Fuel Properties

Parameter	Value	Unit
Coolant Pressure	15.5	MPa
Initial Plenum Pressure	3.1	MPa
UO_2 Density	95%	T.D.

The two smeared cracking models are expected to behave somewhat differently as they calculate the reduction of the fuel elastic properties according to different criteria. Because of the statistical application of the fracture strength to the fuel, several additional simulations have been performed to quantify the variation in the fuel diameter as result of this method.

In total, sixteen simulations were performed; four each for both of the smeared cracking models, with and without the fuel relocation model enabled. Figure 14 shows crack patterns that form by using the exponential-release model (Fig. 14(a)) and the power-release model (Fig. 14(b)) near the end of the simulations. This illustration shows the remaining elastic fuel properties in the azimuthal (hoop) direction as a result of the formation of perpendicular, radially-oriented cracks. Because of how quickly the elastic modulus is reduced, the exponential-release model shows fewer but more well-defined radially cracks. This agrees well with the geometric assumptions used to generate the discrete crack geometry. The power-release model, however, shows a much more diffuse reduction in elastic properties in the fuel periphery, and the crack penetration length into the fuel is shorter. Interestingly, the power-release model indicates the likely formation circumferentially-oriented cracks form during sharp reductions in power

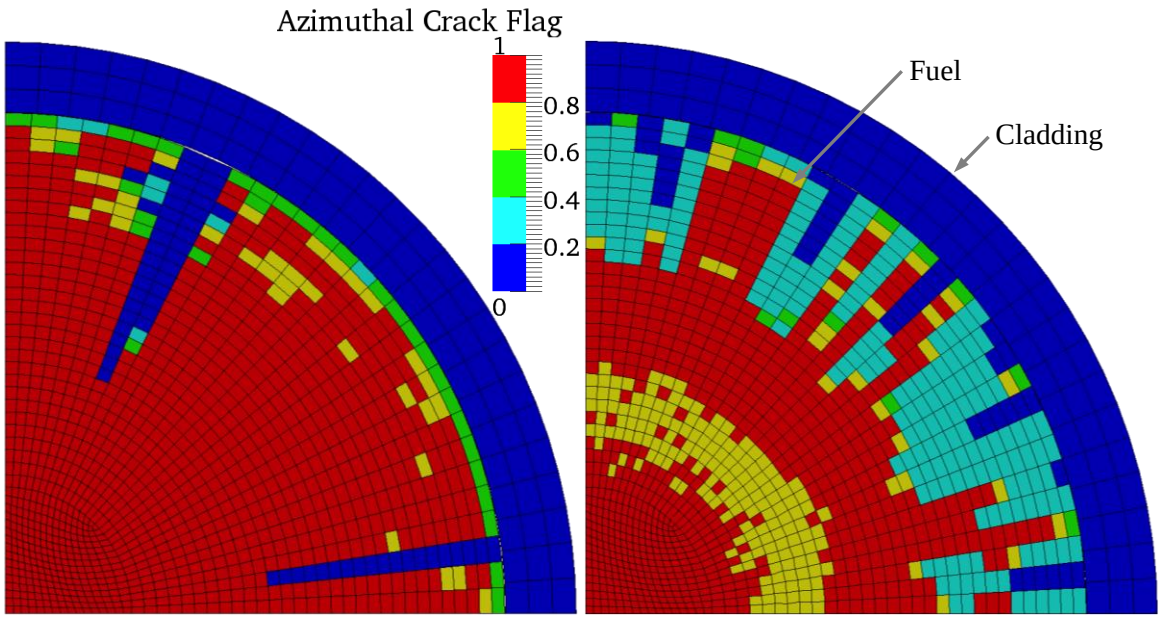

Figure 14. The exponential release model (a) shows fewer cracks that are more well-defined and penetrate further into the fuel radius. The power-release model (b) shows a more diffuse reduction in the fuel elastic properties in the fuel periphery. The plot legend, the azimuthal crack flag, shows the remaining elastic properties in the circumferential direction; the lower the value, the more crack-like the element becomes.

The maximum radial expansion of the fuel (a) and the cladding (b) are shown in Figure 15. The fuel and cladding displacements are both greatly reduced without using fuel relocation. Multiple simulations are performed here to demonstrate the variation in the fuel expansion from cracking due to the statistic application of the fracture strength. Simulations using the power-release smeared cracking model show more fuel expansion and thus more cladding expansion by the end of life the exponential-release model. As well, there is a clearly discernable difference between the fuel expansion based on the application of the fuel relocation model, showcasing that fuel relocation is a dominant expansion contribution. The power-release smeared cracking model also consistently demonstrates significantly more expansion than the exponential release model after fuel densification occurs. By the end of life, there is an approximately 5μm deviation among the fuel expansion profiles based on crack type resulting from the statistical difference in crack formation. Before gap closure occurs, the cladding radius initially increases as the temperature is raised to operating temperature and quickly begins to decrease due to creep deformation from the pressure differential between the internal gas and the system pressure. After the onset of gap closure, the cladding radial expansion plotted in Figure 15(b) shows a deviation similar to the fuel based on the difference in fuel expansion from the cracks. Here, the power-release model shows the least cladding creep down amongst the different models, however, the predicted radial inward displacement is ~20μm greater than the measured radial expansion. It should be noted that the cladding radial expansion measurement is at room temperature, thus, it is compared to the radial displacement at the end of these simulations.

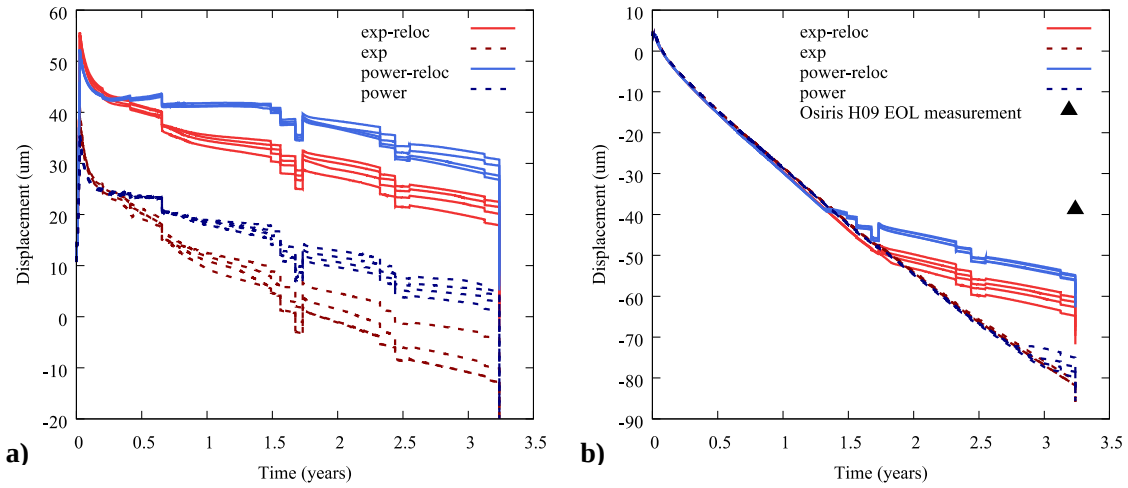

Figure 15. The fuel (a) and cladding (b) radial expansion, as a function of time following the power profile shown in Figure and comparing different fuel mechanics models. The experimental cladding displacement after operation is shown with the black triangle.

Because of the larger (~10μm) fuel expansion for the power-release model over the exponential-release model, it is considered to be in better agreement with the cladding deformation measurement. For the forthcoming analysis, only the power-release model is considered where a smeared cracking model is used.

The fuel centerline temperatures for the OSIRIS H09 test fuel rod for the various fuel mechanics are shown in Figure 16. These results include: the elastic fuel properties, fuel creep deformation, the power-release smeared cracking model (Section 2.2), discrete meshed cracks (Section 2.3), and the isotropic softening model (Section 2.4). Additional simulations are included here without the fuel relocation model for the smeared and discrete cracking models. The variation among the fuel centerline temperatures is almost entirely due to the difference in the gap closure behavior of these fuel rods. The fuel temperatures for smeared cracking, creep, and isotropic softening models only differ a small amount initially until gap closure occurs. Because the discrete cracks are 70% of the fuel radius and included in the simulation at the beginning, they allow the fuel to expand more than the other simulations even before fracture would occur. A smaller fuel cladding gap leads to lower fuel temperatures. Eventually, however, the fuel temperatures begin to converge as gap closure occurs in all fuel rods with relocation before 1.5 years. The fuel rods without relocation show considerably higher fuel centerline temperatures, which are caused by their larger fuel cladding gap size.

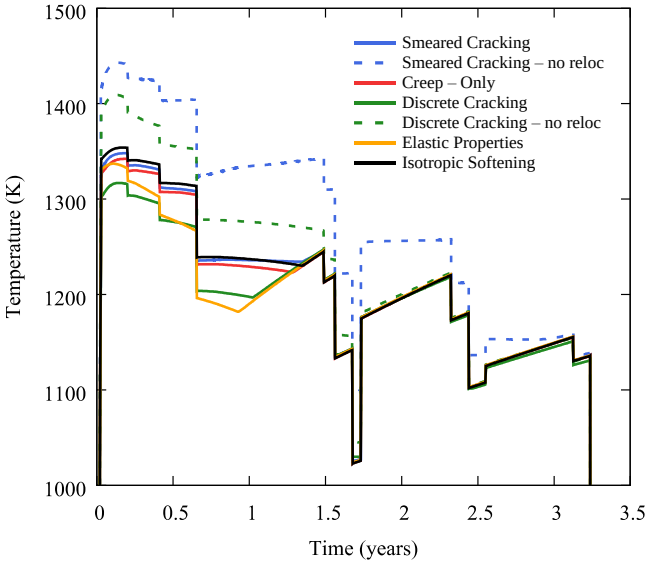

Figure 16. The fuel centerline temperature variation as a function of time as predicted by the various fuel mechanics model simulations.

Figure 17 shows the fuel radial expansion (a) and fuel rod gap thickness (b) variation amongst the different models as a function of time. Because the discrete meshed cracks are essentially fully-developed cracks, they expand more than the fracture models. After densification, the elastic fuel continues to expand from fission product swelling and fuel relocation, resulting in a much larger (>40μm) difference in the final fuel radius than the other simulations. By the end of the simulation, there is an ~10μm difference between fuel radius for the fracture models. Because the smeared cracking model implements a reduction in elastic properties corresponding to circumferential cracks, the fuel expands less than in the isotropic softening and creep-only simulations. In future iterations of these simulations, a crack healing criterion might need to be incorporated to regain the elastic properties under certain compressive stress conditions.

Similarly, gap closure occurs earliest for the fuel rods with the greatest fuel expansion. After the initial fuel expansion caused by fuel thermal expansion and densification, the fuel rod gap closes much faster than the fuel expands. This indicates that the gap closure behavior for these fuel rods is dominated by creep-down of the Zircaloy cladding. This is consistent with results reported previously (Sweet et al., 2018).

Without the relocation model the onset of gap closure is significantly delayed, especially for the smeared cracking where gap closure occurs at ~3 years. As the reactor is shutdown at the end of these simulations, the fuel contracts and the gap is reopened.

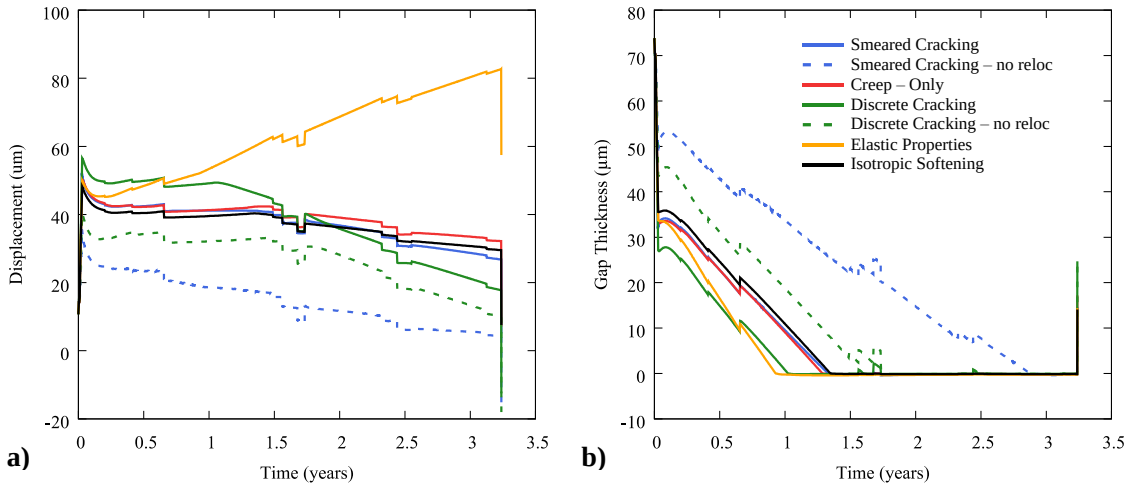

Figure 17. The fuel radial expansion (a) sharply increases initially due to thermal expansion and begins to decrease due to fuel densification where it remains relatively constant until gap closure. The gap thickness (b) sharply decreases early in the simulations until gap closure occurs.

The fuel hoop stress is very sensitive to the constitutive models used in each simulation. Figure 18 shows the fuel hoop stress over the initial rise to operating power (a) and over the full simulation. (b). The behavior of these mechanics models are best described during the rise to power. Because the elastic fuel has no stress relief due to fracture or creep, the stresses continue to increase as the temperatures increase to a steady state at operating power and fuel densification begins. As the hoop stresses increase, the fuel creep model eventually reaches a stress regime where it is sensitive and begins to deviate. After the operating temperature is reached, the stress is rapidly relieved.

The maximum hoop stresses for both smeared cracking models fluctuate near the fuel fracture strength as radial cracks form. Similarly, after the operating temperature is reached the hoop stress is relieved due to creep deformation. The isotopic softening model at the peak linear heat rate features ~7 cracks. Because the elastic properties are reduced isotropically, the hoop stress is almost immediately reduced and shows very little variation over the rest of the operation. Likewise, because the discrete meshed cracks are able to immediately expand, there is very little build up in the hoop stress.

Fig. 18(b) shows the hoop stress profiles over the entire 4 cycles of operation. This emphasizes the impact that the fuel creep and fracture models have on the fuel stress state when compared to the elastic fuel approximation. Because the elastic fuel does not include fuel creep of a fracture model to provide stress relief, the hoop stress is determined by the radial expansion. The strain from relocation is introduced as a stress-free strain, thus the hoop stress is generated by a combination of expansion from the fission product swelling and thermal strain. As such, the hoop stress in the elastic fuel cycles with the variation in the linear heat rate.

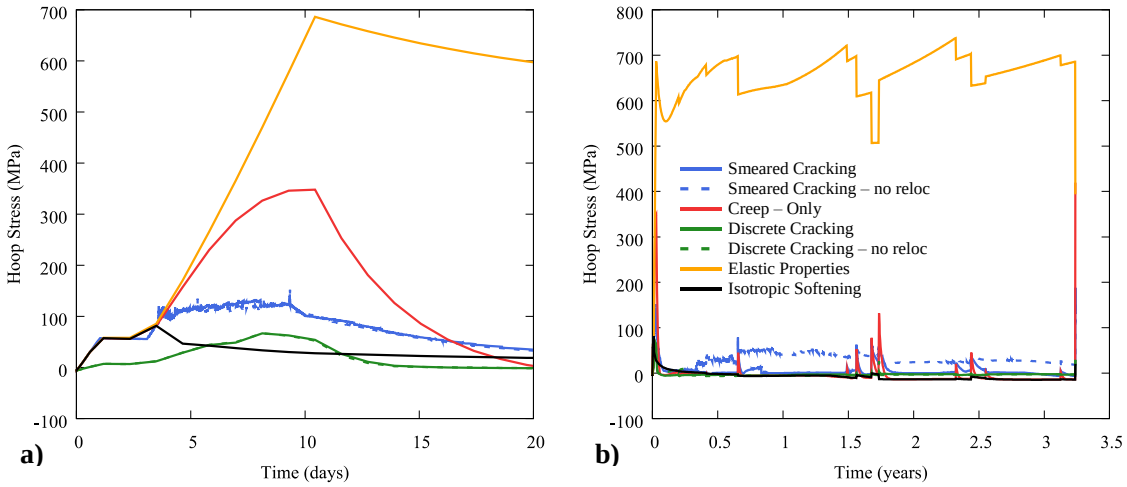

Figure 18. The fuel hoop stress over the first 20 days (a) reaches a maximum at the end of power ascension and slowly decays due to fuel densification and fuel creep. Fuel hoop stresses fluctuate over the full four-cycle (b) operation because of the power swings.

Features in the hoop stress profiles for the fracture models are better visualized by focusing on the lower hoop stress magnitudes, as shown in Figure 19. Immediately after large stresses are induced from fuel power cycling, the fuel creep model allows the fuel to deform and relive the stresses. Because the smeared cracking model can quickly reduce the elastic properties in a single fuel finite-element, stress concentration can form in the fuel. This can artificially increase the maximum hoop stress that is reported in the fuel, as the crack slowly progresses. This can be seen at nearly 0.75 years where the hoop stress is increased without any shift in the fuel temperatures.

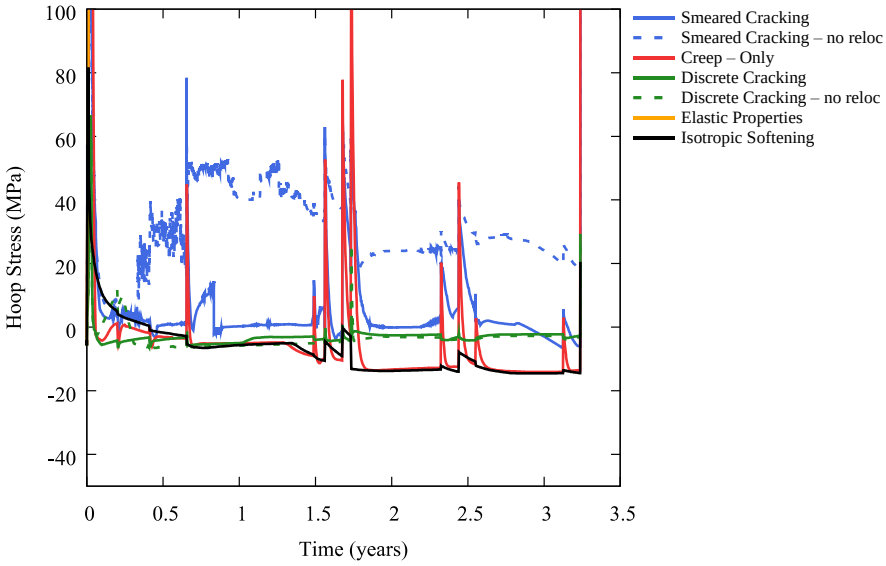

Figure 19. The maximum fuel hoop stress varies by the fracture model due to its behavior during the large shifts in power as prescribed by the power history.

As the cladding temperature increases during the rise to operating power, the cladding radius thermally expands by ~5 µm. Figure 20 shows the cladding radial expansion (a) and the maximum cladding hoop stress (b) for these simulations. Almost immediately, the cladding begins to creep-down due to the pressure differential between the coolant system and the rod internal pressure. The cladding radially expands as mechanical contact occurs for the elastic fuel first. Because the elastic fuel continues to expand, the cladding displacement continually increases. As gap closure occurs in the remaining simulations, the cladding slowly restricts the fuel. The fuel radius is slowly reduced as the linear heat rate is diminished at the end of the simulation. At the end of the operation, all of the fracture models predict significantly more inward displacement (~15 to 40 µm) as compared to the EOL experimental test rod measurement.

After the increase to operating temperature, the Zircaloy cladding is initially in a compressive state until gap closure occurs. Again, fission gas release plays little to no role in the plenum pressure calculations from these fuel rods because there is no discrete fuel plenum volume/temperature calculation. Figure (b) shows the cladding hoop stress for these simulations. After gap closure occurs, only the elastic fuel simulation reaches tensile cladding stresses for any appreciable time, and even these only reach a maximum of ~60 MPa. The other simulations fluctuate in a compressive state after gap closure due to the thermal cycling of the fuel. As the fuel contract during reactor shutdown, the stress rapidly increases reaching a maximum value of ~20 MPa for the isotropic softening simulation.

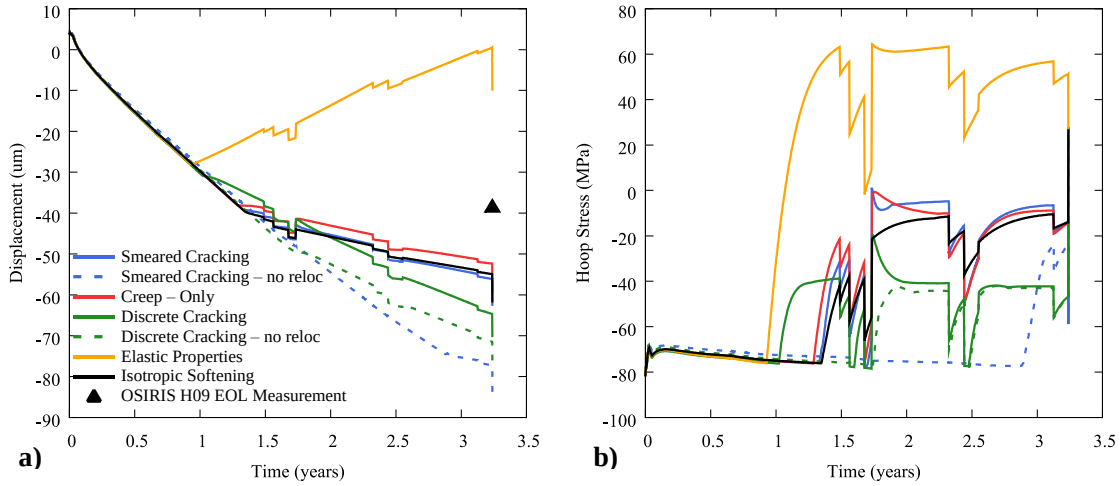

Figure 20. The cladding radial displacement (a) decreases due to creep-down from the pressure differential across the cladding until gap closure occurs. Similarly, the maximum cladding hoop stress (b) is increased after gap closure but remains in a compressive state for many of the simulations for the remaining operation.

These results show an early attempt to reconcile fracture into fuel performance simulations and determine the accuracy of several proposed models against measured fuel rod data. The smeared cracking model implemented here has several assumptions that need to be investigated more closely including the applicability of the model for plane-strain geometries and how the reduction in the elastic modulus should affect the creep compliance of the fuel. Although these results do not provide a great enhancement in the agreement with the measured data, they do provide a framework that can eventually be calibrated and improved for application to different fuel rod geometries and materials.

4. FeCrAl Cladding Results

The goal behind the investigation of the fuel mechanics models was to determine the accuracy of these models using a controlled experiment. Ultimately, this is performed to identify areas where these models can be improved in order to accurately simulate nonconventional fuel geometries with alternative cladding materials. This section discusses the work performed by applying these models, as they are implemented in Section 3, to FeCrAl cladding using the fuel geometry and conditions representative of a BWR.

Figure 21 shows the fuel mesh generated using the specifications summarized in Table 3. For this analysis, the FeCrAl geometry and reactor conditions from the previous Peach Bottom BWR (Table 4) analysis (Sweet et al., 2018) are used in conjunction with the power history from the OSIRIS H09 test rod.

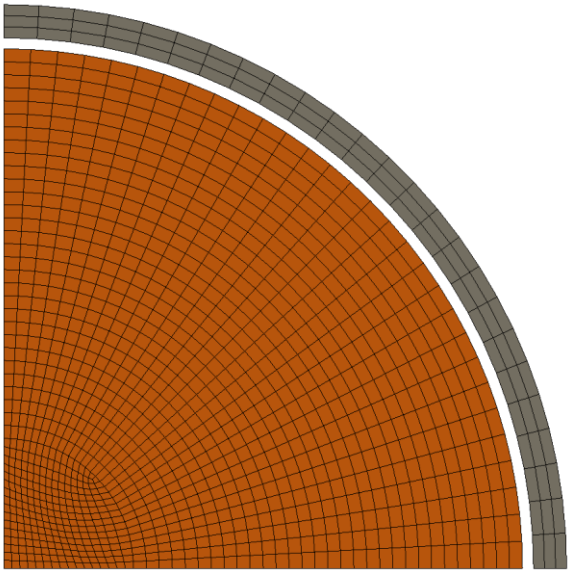

Figure 21. An r-theta fuel rod geometry using specifications from the earlier BWR analysis for the Peach Bottom BWR is used in this analysis.

Table 3. FeCrAl Fuel Geometry Specifications

Cladding Type	Fuel Radius (μm)	Gap Thickness (μm)	Cladding Thickness (μm)
FeCrAl	4700	100	300

Unlike Section 3, BWR conditions are used in the analysis performed here. The large difference here is the initial plenum pressure and the coolant system pressure. The previous analysis used a coolant pressure of 15.5 MPa and a fuel rod plenum pressure of 3.1 MPa. Because there is no effect from the fission gas release model on the fuel rod plenum evolution for these simulations, the plenum pressure remains relatively low for the reactor operation.

Table 4. Boiling Water Reactor and Fuel Properties

Parameter	Value	Unit
Coolant Pressure	7.136	MPa
Coolant Temperature	560	K
Initial Plenum Pressure	.5	MPa
UO_2 Density	95%	T.D.

The fuel centerline temperatures are shown in Figure 22, and demonstrate that the FeCrAl cladded fuel rods behave much differently than the Zircaloy counterparts (discussed in Section 3). In these simulations, the fuel cladding gap does not close. Interestingly, it is the discretely cracked fuel pellet simulation which exhibits the most fuel expansion and thus the lowest fuel centerline temperatures. The simulations without fuel relocation, as expected, show much larger temperatures than their counterparts. Generally, the other simulations share similar behavior with the exception of the smeared cracking model. After the first large drop in power at about 0.6 years, the smeared cracking model shows noticeably less fuel expansion. This occurs because elements are determined to be cracked near the core of the fuel, similar to the crack pattern shown in Fig. 14(b). Because so many of these elements lose their radial strength, as temperatures increase in the core of the fuel, the fuel in these regions lose the ability to exert force on the fuel periphery and further expand the fuel.

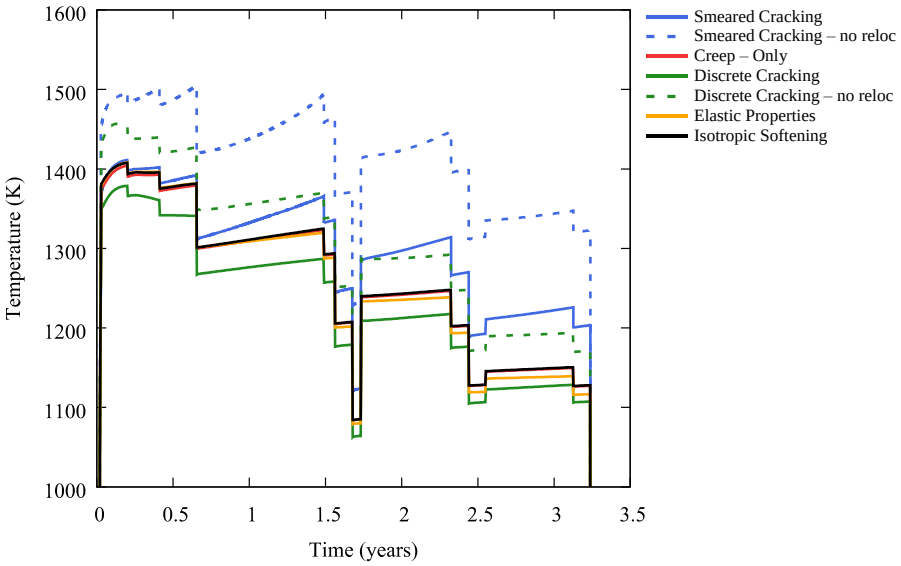

Figure 22. The fuel centerline temperature variation as a function of time as predicted by the various fuel mechanics model simulations. Over these simulations, the smeared cracking simulations show a much higher temperature.

Figure 23 plots the maximum fuel hoop stress (a) and maximum radial displacements (b), respectively. These simulations show a similar maximum hoop stress response over the reactor operation to the Zircaloy cladding. The elastic fuel simulation retains extremely large hoop stresses throughout the simulation, and the other simulations only experience large hoop stresses during large power cycles.

The fuel radial expansion (Fig. 23(b)) also shows a different trend than the Zircaloy cladded fuel rods. The discrete cracked mesh exhibits more fuel expansion earlier in life and retains this expansion through the simulation. The other simulations show similar fuel expansion until the first decrease in power. As

previously mentioned, at this point the fuel expansion in the smeared cracking simulations is significantly hindered.

The simulations without fuel relocation and their counterparts show similar trends, indicating that the magnitude in fuel relocation for these simulations is ~20µm and that the fuel relocation does not change the expansion rate. This implies that the fuel expansion is largely due to fission product swelling, as the fuel continually expands while the fuel temperatures are reduced.

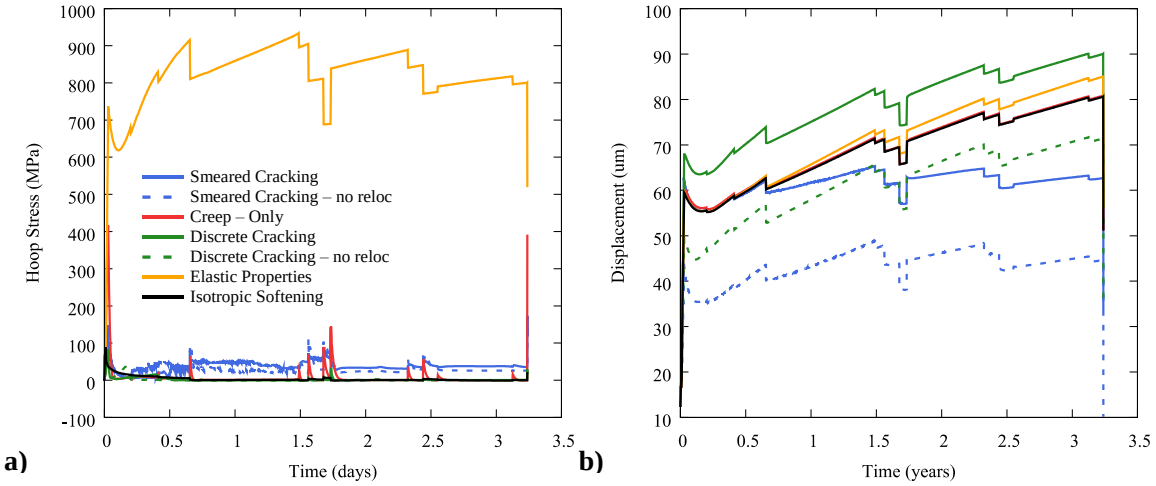

Figure 23. Similar to the previous analysis in Section 3, the maximum hoop stress in the fuel (a) shows spikes corresponding to large power shifts. The fuel radial expansion (b) shows a large variation between models over the four-cycle simulations.

The gap thickness for the FeCrAl cladded fuel rods is shown in Figure 24. Unlike the Zircaloy, the gap does not close quite as rapidly for the FeCrAl cladded fuel rods due to cladding creep down. While there is some creep-down due to irradiation creep in the cladding, fuel expansion dominates the gap closure behavior for these fuel rods. As previously discussed, the smeared cracking models begin to deviate after an early (~.6 years) power cycle in power and exhibits relatively little fuel expansion from that point forward. Because the discrete cracks are meshed into the fuel geometry at the beginning of the simulation, the fuel is rapidly allowed to expand which continue through much of the fuel lifetime.

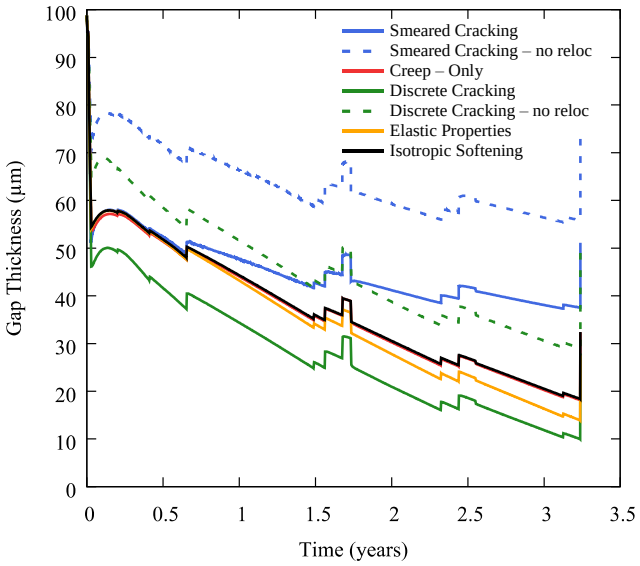

Figure 24. After the initial rise to power, the gap closure behavior varies widely by the model used, however all simulations show sharp variation according to the fuel temperatures.

Because the gap closure behavior of these fuel rods is much different than the Zircaloy rods reported in Section 3, the gap remains open. These results show the sensitivity of the fuel to these fracture models without gap closure, emphasizing that calibration of these models is needed for the uniquely performing alloys with non-conventional fuel geometries. This difference in fuel rod behavior demonstrates the need to develop specific test cases that not only demonstrate the power cycling that an LWR is expected to experience, but also irradiate the fuel long enough to gauge the conditions of interest. Because the FeCrAl cladded fuel rods can exhibit the onset of gap closure much later in life, the greatest effect of the fuel fracture models is on the fuel temperatures. While the variations in predicted fuel temperatures are within ~25K initially, by the end of the simulation the temperatures show an ~100K difference. This is expected to change the fission gas behavior and possibly initiate the bootstrapping effect between the release rate and temperature, although this will need further investigation in full length fuel rod simulations, since the fuel plenum has not been modeled in these simulations.

5. Application of Constant Operating Conditions

In order to assess the FeCrAl cladding behavior after gap closure and subsequent mechanical interaction with the fuel, additional simulations are currently being performed using constant operating conditions. These simulations use the same fuel geometry used in the previous section, however, the linear heat rate is ramped up to 20kW/m and held constant until the fuel reaches an average burnup of 60 MWd/kgU. Using the smeared cracking model as it is implemented, there was some uncertainty whether the fuel creep model should be disabled as the finite-elements are cracked. For this work, simulations will be performed comparing and further modifying this assumption by reducing the creep contribution based on the ratio of the remaining elastic properties in the fuel.

6. Summary and Future Work

In order to improve the accuracy of fuel performance simulations for nonconventional fuel geometries and alternative cladding materials, an initial investigation of the impact of including various fracture models has been performed and discussed in this report. This investigation includes several different methods for the incorporation of fuel fracture, an important mechanism of diametral expansion, into the fuel performance code.

Fuel fracture has been the focus of this investigation, and it was selected for evaluation because it plays a role in the evolution of the fuel cladding gap closure behavior and the subsequent mechanical interaction that determines the cladding stress state. Because many of the current relations used to determine the fuel expansion are highly empirical data fits from specific fuel tests, a more mechanistic solution is sought. In order to begin this investigation, a smeared cracking model was chosen and modified in the BISON fuel performance code. Although this model still lacks many aspects to develop a meaningful comparison representative of fracture in UO_2, it performs relatively well for Zircaloy cladding. For FeCrAl cladding, on the other hand, due to the reduced creep down of FeCrAl cladding, the impact of varying fracture models appears to be much less sensitive than the case of conventional Zr-alloy rods.

Several critical improvements are needed before this model can see widespread deployment. These include improvements in the range of parameters being scaled along with the elastic modulus, such as the Poisson's Ratio and the fuel thermal conductivity, and model improvements such development of a crack healing mechanism and possibly an augmentation to the fission gas release model.

In the current smeared cracking models, the Poisson's Ratio is calculated based on the fuel properties without any impact from fuel fracture. In order to improve the behavior of elements as they are stretched due to crack opening and closing, the Poisson's Ratio should decay using a similar method to the elastic modulus. Likewise, fuel relocation tests show that the onset of cracking is accompanied by a reduction in the thermal conductivity of nearly 30% for the fuel (Williford et al., 1980). Future work on this model will include a calibrated reduction for both smeared cracking and the Poisson's Ratio for the cracked elements.

Future crack models may need to constrain the crack direction and include crack healing. Crack healing is an important aspect of the fracture mechanics affecting re-cohesion or re-sintering of the cracked surface and may result in better agreement with the experimental results as elastic properties are able to be regained. These simulations do not currently include any expedited crack healing model, and as such they cannot exhibit the fuel "ratcheting" associated with continued power cycling. In order to include this contribution to the diametral expansion, crack healing criteria will need to be developed and implemented into the smeared cracking model.

As well, additional work may be performed to incorporate aspects from the fuel fracture model into the fission gas release model. As crack networks propagate both radially and circumferentially through the fuel pellet, new free surfaces are created which may serve as sites to allow more gaseous fission products to diffuse from the fuel (Pastore et al., 2013). Although this fission gas release mechanism has never been thoroughly evaluated through experiments, it is expected to play a role in the transient fission gas release occurring during reactor power maneuvering (Maki and Meyer, 1978).

As well, additional analyses are needed to further identify the cladding stress development due to mechanical contact between cladding and fuel cracks. Localized increases in cladding stress due to PCMI in the presence of fuel cracks and defects have been documented (Capps et al., 2016). To reproduce this

analysis with smeared cracking models, the mechanical contact model currently employed in BISON will have to be investigated to include the effect of friction after gap closure.

Mechanistically modeling the effect of fuel fracture is difficult because of the limited available experimental data that exclusively investigate fuel behavior. By using data from integral fuel rod experiments, error is introduced through inaccuracies in the cladding behavioral models. This presents a unique and difficult challenge suited for continued improvement using high-fidelity fuel performance analysis. Accurately modeling stress evolution in the fuel is key to assessing fuel behavior up to gap closure and the subsequent deformation of the cladding due to PCMI.

7. References

Capps, N., Montgomery, R., Sunderland, D., Pytel, M., Wirth, B.D., 2016. Evaluation of missing pellet surface geometry on cladding stress distribution and magnitude. Nucl Eng Des 305, 51-63.

Cunningham, M., Williford, R., Hann, C., 1979. Effects of fill gas composition and pellet eccentricity: comparison between instrumented fuel assemblies IFA-431 and IFA-432. Battelle Pacific Northwest Labs., Richland, WA (USA).

Gittus, J.H., 1972. Theoretical analysis of the strains produced in nuclear fuel cladding tubes by the expansion of cracked cylindrical fuel pellets. Nucl Eng Des 18, 69-82.

Hagrman, D.T., Allison, C.M., Berna, G.A., 1995. SCDAP/RELAP5/MOD 3.1 code manual: MATPRO, A library of materials properties for Light-Water-Reactor accident analysis. Volume 4.

Hales, J., Novascone, S., Pastore, G., Perez, D., Spencer, B., Williamson, R., 2014. BISON theory manual: The equations behind nuclear fuel analysis. Fuels Modeling & Simulation Department, Idaho National Laboratory, Idaho Falls, Idaho.

Jankus, V., Weeks, R., 1972. LIFE-II—A computer analysis of fast-reactor fuel-element behavior as a function of reactor operating history. Nucl Eng Des 18, 83-96.

Liu, W., Rashid, J., 2017. Continued Improvements in Numerical/Mechanical BISON Models, CASL Milestone Report: L3_FMC_FUEL_P15_08.

Maki, J.T., Meyer, J.E., 1978. LWR fuel performance analysis: fuel cracking and relocation. MIT Energy Laboratory.

Oguma, M., 1983. Cracking and Relocation Behavior of Nuclear-Fuel Pellets during Rise to Power. Nucl Eng Des 76, 35-45.

Olander, D.R., 1976. Fundamental aspects of nuclear reactor fuel elements. California Univ., Berkeley (USA). Dept. of Nuclear Engineering.

Pastore, G., Hales, J., Novascone, S., Perez, D., Spencer, B., Williamson, R., 2013. Analysis of fission gas release in LWR fuel using the BISON code. Idaho National Laboratory (INL).

Rashid, Y., 1974. Mathematical modeling and analysis of fuel rods. Nucl Eng Des 29, 22-32.

Rashid, Y., Dunham, R., Montgomery, R., 2004. Fuel analysis and licensing code: FALCON MOD01. EPRI Report 1011308.

Rashid, Y.R., 1968. Ultimate strength analysis of prestressed concrete pressure vessels. Nucl Eng Des 7, 334-344.

Sartori, E., Killeen, J., Turnbull, J., 2010. International Fuel Performance Experiments (IFPE) Database. OECD-NEA.

Sweet, R.T., George, N.M., Maldonado, G.I., Terrani, K.A., Wirth, B.D., 2018. Fuel performance simulation of iron-chrome-aluminum (FeCrAl) cladding during steady-state LWR operation. Nucl Eng Des 328, 10-26.

Swiler, L.P., Williamson, R.L., Perez, D.M., 2013. Calibration of a Fuel Relocation Model in BISON. Sandia National Laboratories (SNL-NM), Albuquerque, NM (United States).

Walton, L., Husser, D., 1982. Fuel pellet fracture and relocation. FUEL ELEMENT PERFORMANCE COMPUTER MODELLING, 147.

Williamson, R.L., Hales, J.D., Novascone, S.R., Tonks, M.R., Gaston, D.R., Permann, C.J., Andrs, D., Martineau, R.C., 2012. Multidimensional multiphysics simulation of nuclear fuel behavior. J Nucl Mater 423, 149-163.

Williford, R., 1982. Experimental Verification of a Cracked Fuel Mechanical Model. Pacific

Northwest National Laboratory (PNNL), Richland, WA (United States).
Williford, R., Mohr, C., Lanning, D., Cunningham, M., Rausch, W., Bradley, E., 1980. Analysis of fuel relocation for the NRC/PNL Halden assemblies IFA-431, IFA-432, and IFA-513. Pacific Northwest Labs., Richland, WA (USA).